J Membrane Biol (2013) 246:927–938
DOI 10.1007/s00232-013-9594-z

Nanosecond Electric Pulses Affect a Plant-Specific Kinesin at the Plasma Membrane

Sebastian Kühn · Qiong Liu · Christian Eing · Wolfgang Frey · Peter Nick

Received: 13 May 2013 / Accepted: 7 September 2013 / Published online: 24 September 2013

Abstract Electric pulses with high field strength and durations in the nanosecond range (nsPEFs) are of considerable interest for biotechnological and medical applications. However, their actual cellular site of action is still under debate—due to their extremely short rise times, nsPEFs are thought to act mainly in the cell interior rather than at the plasma membrane. On the other hand, nsPEFs can induce membrane permeability. We have revisited this issue using plant cells as a model. By mapping the cellular responses to nsPEFs of different field strength and duration in the tobacco BY-2 cell line, we could define a treatment that does not impinge on short-term viability, such that the physiological responses to the treatment can be followed. We observe, for these conditions, a mild disintegration of the cytoskeleton, impaired membrane localization of the PIN1 auxin-efflux transporter and a delayed premitotic nuclear positioning followed by a transient mitotic arrest. To address the target site of nsPEFs, we made use of the plant-specific KCH kinesin, which can assume two different states with different localization (either near the nucleus or at the cell membrane) driving different cellular functions. We show that nsPEFs reduce cell expansion in nontransformed cells but promote expansion in a line overexpressing KCH. Since cell elongation and cell widening are linked to the KCH localized at the cell membrane, the inverted response in the KCH overexpressor provides evidence for a direct action of nsPEFs, also at the cell membrane.

Keywords BY-2 · Cytoskeleton · KCH kinesin · Membrane · *N. tabacum* · nsPEFs

Abbreviations

nsPEFs	Nanosecond pulsed electric fields
KCH	Kinesin with calponin homology
PI	Pulsing index

Introduction

Research on intense pulsed electric fields (PEFs) can be dated back to the late 1950s (Staempfli 1958), and since then the potential application of PEFs has been explored intensively for various applications, ranging from food pasteurization (Qin et al. 1996) to delivery of macromolecules (Belehradek et al. 1993), including genetic materials (Chang and Reese 1990), extraction of cellular contents (Brodelius et al. 2005), the treatment of certain types of cancer (Weaver and Chizmadzhev 1996) and a dramatic stimulation of mushroom growth via unknown mechanisms (Takaki et al. 2007). The effect of PEF treatment depends on environmental factors, innate characteristics of the specimen and the composition of the media (Alkhafaji and Fraid 2007). However, the mode of application, i.e., the

S. Kühn (✉) · Q. Liu · P. Nick
Botanical Institute, Karlsruhe Institute of Technology, Kaiserstr. 2, 76128 Karlsruhe, Germany
e-mail: sebastian.kuehn@kit.edu

Q. Liu
e-mail: liuqionglandmail@gmail.com

P. Nick
e-mail: peter.nick@kit.edu

C. Eing · W. Frey
Institute for Pulsed Power and Microwave Technology, Karlsruhe Institute of Technology, Eggenstein-Leopoldshafen, 76344 Karlsruhe, Germany
e-mail: christian.eing@kit.edu

W. Frey
e-mail: wolfgang.frey@kit.edu

combination of field strength, pulse duration and number of pulses, is crucial, as summarized by Tang et al. (2009).

Longer pulses with lower field strength lead to reversible pore formation and can induce membrane passage of macromolecules, whereas shorter pulses with higher field strength cause intracellular electromanipulation (Beebe et al. 2002; Buescher and Schoenbach 2003) and are effective at altering cellular functions. For instance, intermediate combinations of pulse duration and field strength can induce apoptosis, which has been exploited for the successful treatment of skin cancers (Nuccitelli et al. 2006, 2009). Ultrashort nanosecond PEFs (nsPEFs) are thought to penetrate into the cell interior and to affect intracellular membranes or organelles before being dissipated by charging of the cell membrane (Chen et al. 2006; Schoenbach et al. 2001, 2004; Gowrishankar et al. 2006). Therefore, it is to be expected that the shorter the duration of the electrical pulse, the more it will act in the cell interior. In fact, rupture of intracellular granules or vacuoles without detectable electroporation to the outer membrane (Schoenbach et al. 2004; Tekle et al. 2005) or calcium release (Beebe et al. 2003; Buescher and Schoenbach 2003) was observed in mammalian cells exposed to nsPEFs. This contrasts with changes of plasma membrane permeability explained by the formation of nanopores (Hu et al. 2005; Gowrishankar et al. 2006; Flickinger et al. 2010). Recent studies indicate that even with very short pulse durations membrane structures are affected; for instance, even nsPEFs with pulse durations of 10–60 ns can trigger membrane permeabilization (Nesin et al. 2011; Ibey et al. 2011; Breton et al. 2012).

Since cellular structures adjacent to the plasma membrane respond to ultrashort electrical pulses, the membrane-associated cytoskeleton of plant cells could also be a site of action. Cortical microtubules, a plant-specific cytoskeletal array responsible for the directional expansion of plant cells, disorganize and progressively redistribute into mesh-like structures from only 3 min after pulsing. In parallel, actin filaments at the cell cortex disintegrate, and actin bundles tethering the nucleus detach from the periphery and contract toward the nucleus. These early cytoskeletal responses were later followed by a progressive loss of plasma membrane integrity (Berghöfer et al. 2009). When actin was stabilized by either phalloidin (Berghöfer et al. 2009), transgenic expression of the actin-bundling domain of plant fimbrin or inducible expression of the actin-bundling LIM domain of the plant WLIM protein, the plasma membrane became more robust against electric permeabilization as monitored by the uptake of a membrane-impermeable dye, trypan blue (Hohenberger et al. 2011). Imaging of GFP-tagged actin filaments and microtubules by total internal reflection microscopy, a technique based on the very low penetrance (around 50 nm) of an evanescent wave from a total reflected laser beam, has revealed that this part of the plant cytoskeleton is directly adjacent to the membrane (Hohenberger et al. 2011), which is consistent with the concept of a cytoskeletal membrane–cell wall continuum in plants (Pickard 2008). It should be mentioned that nsPEFs were reported to disrupt actin also in melanoma cells, which are key targets for nsPEF-based curative treatment, followed by activation of caspases as central regulators of apoptosis (Ford et al. 2010).

In summary, the theoretical predictions that nsPEFs act preferentially at intracellular targets contrast with observations suggesting a site of action at the plasma membrane. It is difficult to resolve this discrepancy because the experiments were conducted in different systems under different conditions and with different scopes. We therefore addressed this issue in a single experimental system, where the same molecular target was localized either in the cell interior or adjacent to the plasma membrane and where different cellular functions can be assigned to these two subsets of the target.

Recently, we were able to identify such a target molecule: a plant-specific member of the kinesin-14 family containing a calponin homology domain (KCH), which links microtubules and actin filaments (Preuss et al. 2004; Gimona et al. 2002; Korenbaum and Rivero 2002). We have stably transformed a KCH homologue from rice (*Oryza sativa* L.) into the tobacco suspension cell line BY-2 (Frey et al. 2009). Later, the innate KCH homologue of this cell line, NtKCH, could be identified, cloned and overexpressed (Klotz and Nick 2012). The analysis of these overexpression lines along with the phenotype of loss-of-function mutants in rice (Frey et al. 2010) identified two cellular functions and sites of action where KCH kinesins are involved: during interphase, they promote cell elongation (Klotz and Nick 2012); in preparation for mitosis, KCH constitutes a central element of the perinuclear cytoskeletal cage that controls the movement of the nucleus toward the cell center heralding the ensuing cell division (Frey et al. 2010).

The motivation of this study was to define the cellular site of action for nsPEFs. The electric field can penetrate into the cell before it is dissipated by charging of the plasma membrane (Schoenbach et al. 2004), which allows one to manipulate intracellular targets, such as membranes of organelles. This contrasts with observations in both plant (Berghöfer et al. 2009) and animal (Ford et al. 2010) cells, where nsPEFs disrupt the cytoskeleton adjacent to the plasma membrane. Due to differences in size, membrane composition, the organization of the endomembrane system and the tissue context, the parameter ranges for physiological responses to nsPEFs differ [for melanoma cells see Nuccitelli et al. (2006, 2009); for plant cells see Flickinger et al. (2010); for seedlings see Eing et al.

(2009)]. This means that parameter ranges have to be determined for each experimental system individually. We therefore first mapped parameter ranges with respect to various physiological responses for our model system, tobacco BY-2 cells.

After defining a physiological, sublethal parameter range, we used a specific cytoskeletal protein, the unconventional plant kinesin KCH1, as a probe. In this study we measured premitotic nuclear positioning (NP, depending on the perinuclear cytoskeleton) and elongation of the highly vacuolated plant cells (depending on the submembrane cytoskeleton).

When nsPEFs preferentially act in the cell interior, this is expected to interfere mainly with NP and thus mitotic activity, whereas cell elongation as a function dependent on the membrane-bound cytoskeleton should be less affected. When nsPEFs cause direct effects at the membrane, we should observe specific effects on cell elongation that are accompanied by (secondary) NP responses because the tether of the perinuclear cytoskeleton to the membrane-associated cytoskeleton should be disrupted. Since KCH functions in both NP and cell elongation, the effects of nsPEFs should be elevated in a KCH overexpressor line.

Materials and Methods

Cell Lines and Cultivation

For this study, the cell line BY-2 [*Nicotiana tabacum* L. cv bright yellow 2 (Nagata et al. 1992)] was used. For cultivation, a defined number of stationary cells were inoculated into 30 ml of fresh, autoclaved MS-medium (4.3 g/l Murashige and Skoog salts (Duchefa, Haarlem, The Netherlands), 30 g/l sucrose, 200 mg/l KH_2PO_4, 100 mg/l inositol, 1 mg/l thiamine and 0.2 mg/l 2,4-dichlorophenoxyacetic acid, pH 5.8) in a 100-ml Erlenmeyer flask. The volume of the inoculum was adjusted such that the stationary phase was reached at day 7 and ranged between 1.0 and 1.5 ml depending on the batch. The duration of the cultivation cycle was set to 7 days. The suspension was incubated at 25 °C in the dark on an orbital shaker (KS250 basic; IKA Labortechnik, Staufen, Germany) at 150 rpm. As backup, calli were subcultured monthly in the same medium solidified with 0.8 % (w/v) Danish agar (Carl Roth, Karlsruhe, Germany) (Frey et al. 2009). The transgenic BY-2-OsKCH1 cell line was derived from BY-2 cells by stable transformation with OsKCH1 (KCH domain from *O. sativa*) in fusion with GFP under control of a constitutive CaMV 35S promotor (Frey et al. 2009) and maintained in MS-medium under the same conditions but supplemented with 50 mg/l kanamycin as a selective agent to enforce expression of the transgene. The transgenic AtPIN1-RFP line expresses an RFP fusion with the auxin-efflux carrier AtPIN1 under the control of the AtPIN1 promotor (Růžička et al. 2009) and is cultivated in medium supplemented with 100 mg/l kanamycin. Due to slower growth, in this line 3 ml of inoculum have to be used for subcultivation. The BY-2 line AtTuB6 (Nakamura et al. 2004) stably expresses *Arabidopsis* β-tubulin TuB6 fused to GFP under the control of the CaMV 35S promotor and allows life-cell imaging of microtubules while maintaining normal dynamics and organization of microtubules. This cell line was cultivated under the same conditions in medium supplemented with 50 mg/l kanamycin and inoculation of 1.5 ml stationary-phase culture for subcultivation.

The tobacco BY-2 cell line GF11 (Sano et al. 2005) is stably transformed with a fusion of GFP to the fimbrin actin-binding domain 2 under the control of the CaMV 35S promotor and allows visualization of actin filaments in living cells. This cell line was cultivated under the same conditions in medium with 30 mg/l hygromycin and inoculated with 1.5 ml of stationary cells.

Application of nsPEFs

Aliquots of stationary tobacco cells (7 days after subcultivation) were complemented with pulsing buffer (125 mM KCl, 5 mM $CaCl_2 \cdot 2H_2O$, 5 mM $MgCl_2 \cdot 6H_2O$, 150 mM sorbitol and 1 mM Tris, pH 7.2, conductivity 4 mS/cm) with a ratio of 5 volumes of densely packed cells to 3 volumes of buffer. For nsPEF treatment, 1.6 ml of this mixture were used. Electroporation cuvettes (BTX Instrument Division, Holliston, MA) with a rated electrode distance of 4 mm and a volume of 800 µl were used as treatment chambers during all experiments. The field strength (kV/cm) arises from the calculation of 2.5 times the pulse amplitude. Rectangular pulses with pulse amplitudes of 2, 4, 8 and 20 kV were administered, corresponding to field strengths of 5, 10, 20 and 50 kV/cm. Pulse durations of 10, 25 and 100 ns were generated by a transmission line pulse generator (Eing et al. 2009). The 10–90 % pulse rise time of the pulse was $T_r = 2.5$ ns. The electrical energy density (J/cm^3) delivered to the cell suspension was calculated as the product of the square of the field strength, pulse duration, number of pulses and conductance = 4 mS/cm. For simplicity, it was assumed that 1 ml of cell suspension represents a mass of 1 g. For the studies on the potential cellular site affected by nsPEFs in the KCH1 overexpression line, three sets of sublethal treatments were defined as pulsing indices 1–3. Table 1 shows the applied parameter sets for these indices. For all other studies, parameter sets are mentioned in the figure legends or in the figures themselves.

Before each batch of experiments, a test sample of the same suspension was prepared to adjust conductivity and working temperature in order to ensure matched load

Table 1 Pulsing parameters, including pulse duration, number of pulses and electric strength applied, in experiments exploring the potential site of action of nsPEFs in the KCH1 overexpressor line: duration was 25 ns throughout

Pulsing index (PI)	0	1	2	3
Duration time, *T* (ns)	–	25	25	25
Number of pulses, *N*	–	20	10	20
Electric strength, *E* (kV/cm)	–	5	10	10
Energy, *W* (J/kg)	–	50	100	200

conditions to the transmission line generator. After adjusting the pulse generator to the optimal working conditions for the respective parameter sets and samples, the actual probing samples were treated. After pulsing, 1.6 ml of cell suspension from two consecutively pulsed cuvettes were transferred into 30 ml of fresh medium in 100-ml Erlenmeyer flasks supplemented with the respective antibiotics and cultivated as described above. Aliquots of the cells were collected at different time points after pulsing, for phenotypical analysis.

Quantification of Mortality

To determine, how many cells were killed due to the application of nsPEFs, mortality was measured using an assay based on the membrane-impermeable dye Evans blue (Gaff and Okong'O-Ogola 1971). Aliquots of 300 µl of pulsed cell suspension were drained in custom-made staining chambers using a sieve with a mesh size of 70 µm and then transferred into 1 ml of 2.5 % Evans blue (w/v) in MS-medium. After incubation for 5 min, the dye was drained and cells were washed three times for 5 min with fresh medium. Living cells did not take up the dye, whereas dead cells were readily discriminated by intense coloring, as shown in Fig. 1a. At least 2,000 cells for each data point were imaged in differential interference contrast microscopy (AxioImager Z.1; Zeiss, Jena, Germany) using the MosaiX function to ensure unbiased sampling (Zeiss). The cell counter algorithm of ImageJ (http://rsb.info.nih.gov/ij/) was used to quantify the incidence of dead cells.

Mitotic Index

To investigate the proliferation status of the pulsed and nonpulsed BY2 cells, the mitotic index (MI) was measured, as described in Maisch and Nick (2007). The MI is defined as the relative frequency of cells in prophase, metaphase, anaphase and telophase. To discriminate nonmitotic (uncondensed chromatin) from mitotic (condensed chromosomes) cells, the fluorescent dye Hoechst 22358 (Sigma-Aldrich, Neu-Ulm, Germany) intercalating into the DNA was used. For each data point, a sample of 2,000 individual cells from three independent experiments was scored.

Cell Division Synchrony

Cell division synchrony monitors the polar transport of auxin through the cell file and so far represents the most

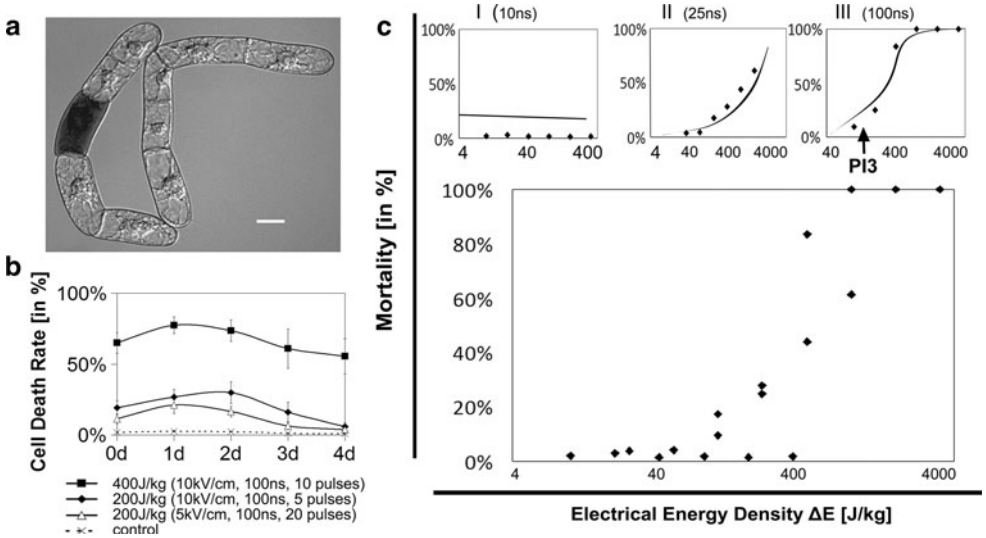

Fig. 1 Mortality in response to nsPEFs. **a** Detection of mortality based on staining with Evans blue. *Scale bar* = 50 µm. **b** Time course of cell mortality after pulsing with different energies. *Values* represent means and standard errors of a population of $n = 2{,}000$ individual cells from three independent experimental series. **c** Mortality for different pulsing parameters plotted over electric energy density, $\Delta E = \sigma E^2 \tau N$, and categorized according to pulse durations of 10 ns (*I*), 25 ns (*II*) 100 ns (*III*) shown in the small charts. *PI3* indicates the scaling parameter used for the investigation of OsKCH1 function throughout this study

sensitive indicator for impaired actin function (Maisch and Nick 2007). To quantify division synchrony, aliquots of cells were collected at defined time points after subcultivation/pulsing, diluted in MS-medium to a density optimal for observation and immediately viewed under an Axioskop or AxioImager Z.1 microscope. Frequency distributions over the number of cells per individual file were constructed (excluding the rare cases with more than ten cells) to assess division synchrony (Campanoni et al. 2003). Each data point represents at least 2,250 cell files from three independent experimental series.

Packed Cell Volume

Growth of the BY-2 cell culture was quantified by measuring the packed cell volume (PCV) as described in Jovanovic et al. (2010) at day 5 or 7 after subcultivation/pulsing. Aliquots of 14 ml of suspension were poured from the Erlenmeyer flasks directly into two 15-ml Falcon tubes (BD Biosciences, San Jose, CA) and kept vertically at 4 °C for a time period between 48 and 72 h (depending on the density of the cell culture) until the supernatant was completely clear, such that the PCV could be directly read out according to the scale of the 15-ml Falcon tube.

Measurement of Cell Length and Width

To detect morphogenetic responses, cell length and cell width were measured at days 1 and 5 after subcultivation/pulsing using the measurement function of the AxioVision Imaging software (Zeiss). At day 1 mitotic activity was maximal, whereas at day 5 cells had completed expansion and entered the stationary phase. Mean values and standard errors (SEs) were calculated from about 500 cells per data point.

Quantification of NP

NP was quantified according to Frey et al. (2010) from images recorded daily by differential interference contrast through days 0–5 after subcultivation/pulsing. The ratio of the shortest distance between the nuclear center and cell width in the central plane was determined using the measurement function of the AxioVision software. A value of 0.5 represents a central position, whereas a value of 0.25 represents a nucleus adjacent to the side wall. For each data point, NP values from 500 cells were recorded to calculate mean values, SE and frequency distributions classified into the following clusters: 0–0.1, 0.11–0.2, 0.21–0.3, 0.31–0.4 and 0.41–0.5.

Oryzalin Treatments

Oryzalin sequesters tubulin dimers and therefore eliminates microtubules depending on their innate turnover. Different dilutions from a 100-μM stock solution of oryzalin (Sigma-Aldrich) in DMSO were added directly after subcultivation, and the effect on growth was assessed by determining the PCV at day 4.

Microscopy and Image Analysis

Mortality, MI and division synchrony were determined using an Axioskop 2 FS microscope (Zeiss) equipped with a CCD (Axio-Cam MRm, Zeiss) digital imaging system and differential interference contrast. Images were acquired by the AxioVision 4.7 software (Zeiss). For the analysis of actin filaments, microtubules and NP, the AxioImager Z.1 microscope was used. This microscope is equipped with an ApoTome microscope slider for optical sectioning and a cooled digital CCD camera (Axio-Cam MRm). GFP fluorescence was recorded through the filter set 38 HE (excitation at 470 nm, beam splitter at 495 nm and emission at 525 nm). For the evaluation of nuclear position, samples were observed in the differential interference contrast using a 20× objective and MosaiX imaging software (Zeiss), which allows automatic imaging of specified small areas of the slide frame by frame, instead of taking individual pictures manually, a procedure that ensures unbiased sampling. Images were analyzed by AxioVision 4.7 software using the length measurement option. Images were processed with Adobe PhotoShop® (Adobe Systems, San Jose, CA).

Results

Mapping the Lethal and Sublethal Ranges of nsPEFs in BY-2 Cells

To map the parameter set for lethal and sublethal ranges of BY-2 cells in response to nsPEFs, different combinations of field strength (5, 10 and 20 kV/cm), pulse duration (10, 25 and 100 ns) as well as pulse number (10 and 20 times) were imposed, yielding total electrical energy densities ranging from 10 to 1,600 J/kg (Fig. 1). The results showed that mortality increased sharply with increasing energy level (Fig. 1b). Doubling the energy from 200 to 400 J/kg resulted in an almost fourfold increase of mortality, from 24.8 to 84.6 %. When the same energy (200 J/kg) was administered with shorter pulses (duration 25 ns), mortality was somewhat lower (compare open triangles with black diamonds in Fig. 1b). For 400 J/kg imposed by pulses of 100 ns, mortality was 83.6 % but only 43.95 % when imposed via pulses of 25 ns. Complete extermination of the

cells was caused by 800 J/kg imposed by pulses of 100 ns; however, when the same energy was provided by pulses of 25 ns, 38.7 % of the cells survived and finally recovered from the shock as indicated by the PCV (data not shown). Pulses with a duration of 10 ns, under our experimental conditions, were not able to cause cell death at all (data not shown). To test at what range reciprocity is valid, mortality was monitored at day 3 after pulsing and plotted over electrical energy density (ΔE)

$$\Delta E = \sigma E^2 \tau N$$

where σ is the conductivity of the suspension, E is the intensity of the electric field, N is the number of pulses and τ is pulse duration (Schoenbach et al. 2009). The result (Fig. 1c) showed clearly that mortality increased with energy density but that the slope of the line was highly dependent on pulse duration. For 10 ns (Fig. 1c, I) there was almost no increase in mortality, even for the high energy densities, for 25 ns the slope was intermediate (Fig. 1c, II) and for 100 ns it was steep (Fig. 1c, III). This suggested that reciprocity holds for constant pulse duration but that pulse duration is more critical as a decisive factor for the extent of the damage.

The time course of mortality (Fig. 1b) showed that in addition to immediate effects of the pulses (scored at day 0, about 2 h after the treatment), mortality increased during the first day after pulsing, with by a gradual decrease during the following days. For 200 J/kg (especially when delivered by pulses of 5 kV/cm), mortality eventually dropped to the residual level found in unpulsed controls. This decline of mortality over time has to be seen in the context of ongoing division of the viable cells, which will increase the total cell number and thus lower the ratio of dead cells. The peak of mortality observed at day 1 after pulsing is composed of those cells that were killed immediately (possibly caused by the membrane permeabilization) represented by the measurement at day 0 and a fraction of cells that had died more slowly in the course of the first day after pulsing. This fraction (most evident for the mild treatments with 200 J/kg) died as consequence of a biological process culminating in cell death in a progressive fashion and bearing a resemblance to programmed cell death.

Cellular Responses to nsPEFs

To understand the nature of cell death in response to sublethal pulsing, we followed various morphological parameters using fluorescently tagged transgenic cell lines generated in a BY-2 background (Fig. 2). We observed that cytoplasmic architecture became stratified, cytoplasmic streaming ceased, the nucleus was displaced toward the cell periphery and the membrane detached from the cell wall within 3–5 h after treatment with 10 pulses of field strength of 10 kV/cm and duration of 100 ns (Fig. 2a–c). At the same time, cells were progressively depleted from actin filaments (Fig. 2d) and microtubules (Fig. 2e). The auxin-efflux carrier PIN that was strictly localized to the cross-walls in unpulsed controls (Fig. 2f, left) assumed a more diffuse localization such that the cross-walls appeared wider (Fig. 2f, right). This loss of membrane localization should impair auxin flow through the cell file, which should become manifest as a reduction in the frequency of a diagnostic peak for hexacellular files and an increase of quadricellular files (Campanoni et al. 2003). In fact, we observed a significant reduction in the frequency of $n = 6$ at a simultaneous increase at $n = 4$ evident even for a mild treatment with 50 J/kg (Fig. 2g) indicative of an impaired auxin flow, corroborating the observed delocalization of the PIN protein (Fig. 2f) (Nick et al. 2009). Cell growth evaluated via PCV measured 7 days after pulsing showed an all-or-none response. Below a threshold, growth was not significantly affected; above this threshold, cells were exterminated completely right after pulsing (Fig. 2h).

Synergistic Effect of nsPEFs and OsKCH1 on Mitosis

Microtubules control premitotic nuclear migration in concert with the minus end–directed kinesin OsKCH1 (Frey et al. 2010). This kinesin exists in two dynamic states, either detached from actin adjacent to the plasma membrane or linked to actin near the nuclear envelope (Klotz and Nick 2012). We therefore investigated the role of nsPEFs on NP (assessed 1 day after pulsing) in the nontransformed BY-2 wild type versus a cell line overexpressing OsKCH1 for pulses of increasing energy as indicated in Table 1. Hereby, a pulsing index (PI) of PI0 represented a sham treatment without pulsing cells, with PI1 representing the lowest (50 J/kg) and PI3 the highest (200 J/kg) energy density. Pulse duration for these treatments was kept constant to 25 ns. In the nontransformed wild type, the control without pulsing produced a value of ~ 0.37, which means that most nuclei had reached the cell center. All three pulse treatments reduced NP by about 30 % (Fig. 3a), already for the lowest energy density. Similarly, the PI0 control value for the OsKCH1 overexpressor was reduced with respect to NP by about 30 % compared to the wild type without pulsing, consistent with previous results (Frey et al. 2010). When the OsKCH1 line was challenged by nsPEFs, this impaired NP even further culminated in a reduction by about 60 % for 200 J/kg, representing a situation where most nuclei had not moved out from their starting position at the cell periphery. Thus, the nsPEFs and the elevated expression of OsKCH1 act synergistically.

To test the persistence of the delay, we followed NP through several days after pulsing for the PI of PI3 (200 J/kg), where the difference between nontransformed wild

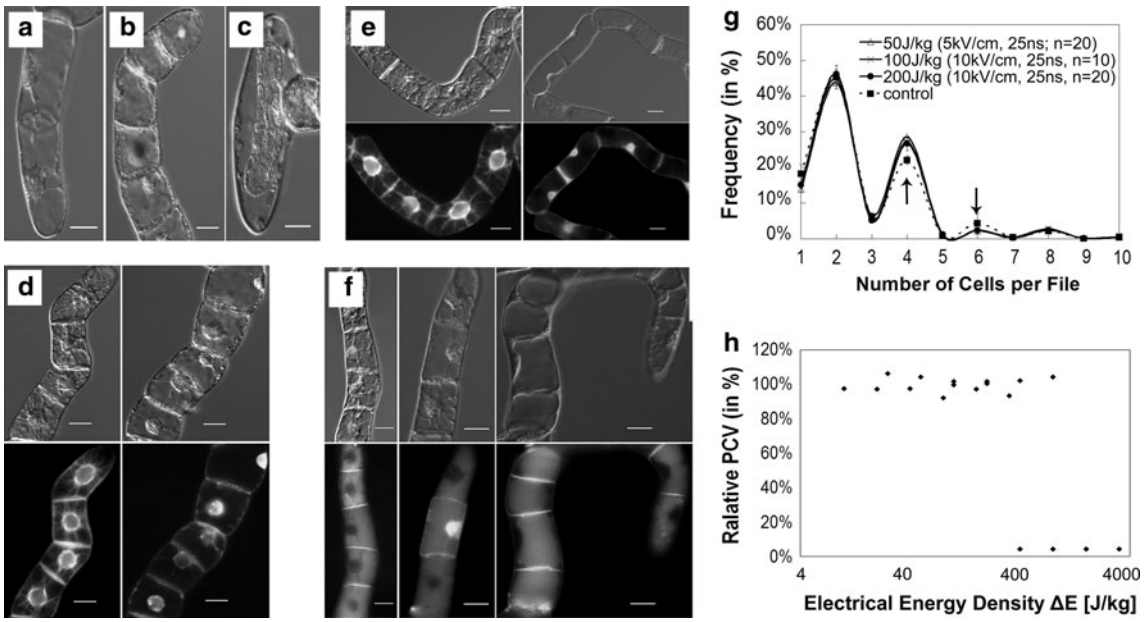

Fig. 2 Cellular responses to sublethal nsPEFs. **a** Vacuolar stratification. **b** Blocked streaming and stratification of cytoplasmic strands. **c** Plasmolysis. **d** Loss of actin structure (*right*) compared to the nonpulsed control (*left*) visualized in the BY2-GF11-GFP cell line. **e** Loss of microtubule structure (*right*) compared to the nonpulsed control (*left*) visualized in the BY2-βTuB-GFP cell line. **f** Delocalization of PIN1 in the BY2-PIN-GFP cell line after pulsing (*right*) compared to unpulsed controls (*left*). Pulsing parameters for **a–f** were $n = 10$, 10 kV/cm and duration 100 ns. **g** Division synchrony can be generally demonstrated by a frequency distribution of the number of individual cells per file. In response to a weak nsPEF (pulsing parameter indicated in the figure) a reduction of the diagnostic peak at $n = 6$ and an increase of the peak at $n = 4$ are manifest (indicated by *arrows*). These changes report an impaired auxin transport in cells pulsed with weak nsPEFs. **h** Packed cell volume determined 7 days after pulsing plotted over electrical energy density, $\Delta E = \sigma E^2 \tau N$. *Scale bars* in **a–f** = 20 µm

type and the OsKCH1 overexpressor was maximal (Fig. 3b). When the wild type was not challenged by a pulse, the nucleus had reached a central position within 1 day and subsequently gradually moved out from the cell center after day 3, when the culture progressed from rapid cycling to a stationary phase. By the pulse treatment, the movement of the nucleus into the cell center was delayed by about 1 day; but eventually the nucleus reached a central position at day 2 after pulsing and then returned to a lateral position at roughly the same time as the unpulsed control. Again, the unpulsed OsKCH1 overexpressor resembled the pulsed wild type. NP was not completed before day 2, and the nuclei did not become as central as in the wild type. Upon pulsing the OsKCH1 overexpressor, NP was even further delayed by an additional day, confirming the synergistic effect of pulsing and OsKCH1 overexpression.

Since NP is a prerequisite for mitosis, we followed in parallel the time course of MI (Fig. 3c) and observed a pattern that was almost identical to that found for NP.

Response of Cell Expansion in BY2-OsKCH1 to nsPEFs Is Inverted

Expansion of plant cells is driven by the osmotic gradient between medium and protoplast, but it is limited by the extensibility of the cell wall. The mechanical properties of the cell wall depend on cellulose texture, which in turn is controlled by a plant-specific subpopulation of the membrane-associated cytoskeleton, the cortical microtubules. Overexpression of the plant-specific KCH kinesin OsKCH1 promoted both cell width (Fig. 4a, c) and cell length (Fig. 4b, d). Approximating volume by a cylindrical shape, the volume of the OsKCH1 overexpressing cells is estimated to excel that of the nontransformed wild type considerably (by a factor of 2.3 at day 1 after inoculation, when mitotic activity ensues, and still a factor of 1.51 after any mitotic activity has ceased at day 5 after inoculation). This difference is even promoted upon pulsing with PI3: now the OsKCH1 overexpressing cells are 3.4 times (day 1) or 2.04 times (day 5) larger compared to the pulsed wild type. The cause for this volume increase is a pronounced stimulation of both elongation and lateral expansion in the OsKCH1 overexpressor during the first day after the pulse (Fig. 4a, b). In contrast, the nontransformed wild type shows reduced lateral expansion and constant length under these conditions. During the subsequent division phase, the length increment caused by cell elongation is counterbalanced by the length reduction in consequence of (axial) cell divisions. Therefore, in both lines, nsPEF treatment caused a reduction in length (Fig. 4d), indicating that cell elongation is

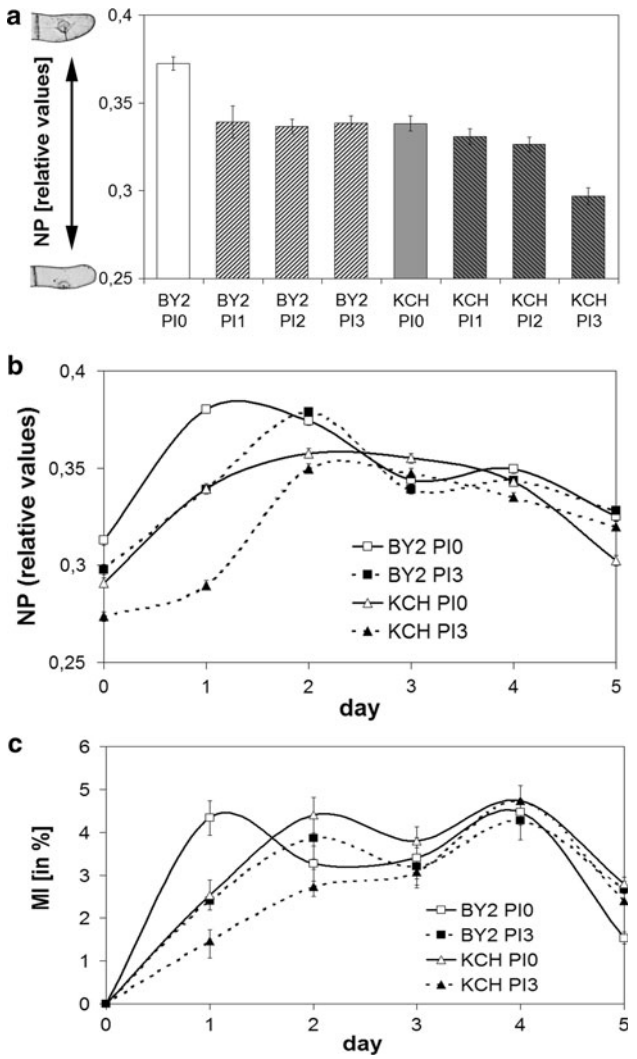

Fig. 3 Synergy of nsPEFs and KCH kinesins in the delay of premitotic nuclear positioning and entry into mitosis. **a** Relative nuclear position (*NP*) values (1 day after pulsing) in relation to nsPEFs of different pulsing indices (*PI*, see Table 1 for parameters, duration was 25 ns throughout). **b** Time course for nuclear positioning for pulsed and nonpulsed BY2-WT (*squares*) and BY2-OsKCH1 (*triangles*) cell lines. **c** Time course of mitotic indices (*MI*) for pulsed and nonpulsed BY2-WT and BY2-osKCH1 cell lines. Data show mean values and standard errors from $n = 1{,}500$ individual cells from three independent experimental series

more sensitive compared to cell division. In contrast, lateral expansion (Fig. 4c) follows the same pattern as observed for day 1 (Fig. 4a), with the general difference that all cells are narrower at day 5 compared to day 1.

The effect of a mild (PI3) nsPEF treatment on cell expansion can therefore be summarized as follows: (1) cell expansion is inhibited in the nontransformed wild type but stimulated in the OsKCH1 overexpressor and (2) cell expansion is more sensitive compared to cell division in both nontransformed wild type and the OsKCH1 overexpressor.

Discussion

This study was motivated by the question of whether it is possible to demonstrate a differential effect of nsPEFs on a molecular target depending on the localization of this target adjacent to the membrane or in the cell interior. A model of our motivation is figured in Fig. 5. We addressed this question by making use of the dual localization of the plant-specific KCH kinesins that convey specific cellular functions (nuclear migration versus cell expansion) that can be assigned to one subset of the target.

In order to adjust the conditions for this experiment, we had first to map the parameters of the pulse treatment such that we remained in the physiological range. Compared with other systems BY-2 cells are relatively sensitive to nsPEFs: lethality is reached at lower energies (10 kV/cm, 20 pulses, 800 J/kg) compared to seedlings of *Arabidopsis thaliana* [50 kV/cm, 10 pulses, 10,000 J/kg (Eing et al. 2009)], although in both cases the duration of pulses is relevant with high lethality for pulse durations of 100 ns. Mammalian tumor cells seem to be far more resistant: Nuccitelli et al. (2006) reported that 100 pulses of 21 kV/cm and 300 ns were required to cause the rapid shrinkage of nuclei in those cells, whereas the application of even 300 pulses of 40 kV/cm and 300 ns could trigger both necrosis and apoptosis in murine melanomas, resulting in complete tumor remission in test animals (Nuccitelli et al. 2009). For the human ovarian carcinoma cell line SKOV3, treatment with 300 electric pulses of 10 kV/cm and 100 ns was needed for significant apoptosis (Yao et al. 2008). From this comparison two conclusions can be drawn: (1) individual cells (whether plant or mammalian) are killed at lower energy densities compared to cells in a tissue context and (2) plant cells are more sensitive compared to their animal counterparts. The first phenomenon can be explained by biology—in a tissue, damaged cells can be replaced by division of their neighbors, which will ensure the survival of the tissue or organism. The second phenomenon can be explained by biophysics: when, for the sake of simplicity, the cell is approximated as a sphere, the local membrane voltage induced by a field is proportional to the radius of the cell, the field strength and the cosines of angle with the field vector (Kotnik and Miklavcic 2000). Since plant cells are considerably larger compared to mammalian cells, the membrane voltage inflicted by a given field is larger and less energy is required to cause a biological effect.

Perception of physical signals such as light, gravity or electrical fields is often an instantaneous process and therefore follows so-called reciprocity: the amplitude of the biological response depends on the total energy of the stimulus, whether this energy is administered by a weak stimulus acting over a longer time or a short stimulus

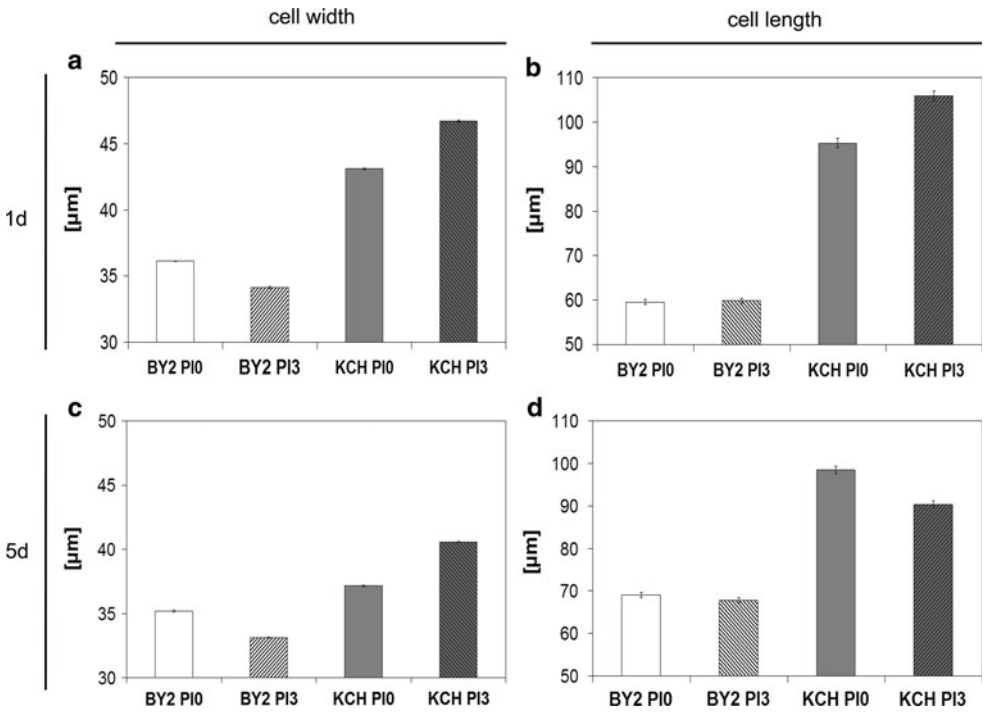

Fig. 4 Response of cell expansion to nsPEFs. **a**, **c** Cell width and **b**, **d** cell length at day 1 (**a, b**) and day 5 (**c, d**) after pulsing in nontransformed (*white bars*) BY2-WT versus BY2-OsKCH1 (*gray bars*) either without pulsing (*blank bars*) or with pulsing using a PI3 treatment (duration 25 ns, *striped bars*). Data represent mean values and standard errors from 500 individual cells from three independent experimental series

acting for a short duration. For photophysiology, this reciprocity has been described by the famous Bunsen–Roscoe law. A bioelectric version of this reciprocity rule has been proposed by Schoenbach et al. (2009), suggesting that the biological response to nsPEFs depends on the electrical energy density, whether this density was established through altered pulse duration, electric field intensity or numbers of pulses. In our study we did not observe reciprocity, but the effects of a given absorbed dose [calculated according to Schoenbach et al. (2009)] varies obviously depending on the parameters of the pulse. The same electrical energy density delivered through combinations of different field intensity and pulse duration could lead to very different results in cell death. Longer pulse duration with lower field strength is more effective at killing BY-2 cells compared to shorter pulse duration with high field strength even when both generate the same electrical energy density. This effect might be linked with the existence of a second large membrane system in plant cells, the tonoplast delineating the vacuole. Since most of the cell interior of expanding plant cells is occupied by a huge vacuole, there exists a second large condensator system of comparable area to the plasma membrane. Depending on the relation between the time constants for charging the plasma membrane [typically in the range 0.1–1 µs (Nuccitelli et al. 2006)] and the tonoplast, different pulse durations are expected to cause different biological effects. Disintegration of the tonoplast is a cellular event that triggers programmed cell death, the plant version of apoptosis. Tonoplast and the plasma membrane differ in their charge, a parameter that is traditionally used in the plant field to purify both membranes differentially by so-called two-phase partitioning.

These considerations show that the differences in the susceptibility of different biological systems to nsPEFs cannot be understood by mere biophysics. Cell biology does matter. Using fluorescently tagged transgenic reporter lines, we therefore searched for cellular targets of nsPEFs. We identified plant-specific arrays of actin filaments and microtubules as sensitive targets that are severely affected by pulses with a duration of 100 ns. A second, highly sensitive target specific for plant cells is the localization as well as dynamics of auxin-efflux carriers that underlie the directional flux of the plant hormone auxin, a central integrator of plant organisms. In our cellular system even small perturbations of these dynamics become manifest as a disturbed synchrony of cell divisions within a cell file, leading to a specific alteration in the frequency of hexacellular files. This specific effect can be deduced from the observed disruption of actin filaments by nsPEFs because actin participates in a cyclic deposition of auxin-efflux carriers (Nick 2010). Since this involves endocytosis that is strongly dependent on actin filaments, at least in plants, our findings are consistent with the previously described phenomenon of "electroendocytosis" (Rosemberg and Korenstein 1997).

The debate, whether nsPEFs cause their biological effect by altering targets at the plasma membrane or by directly perturbing targets in the cell interior has persisted because the experimental evidence derives from different biological

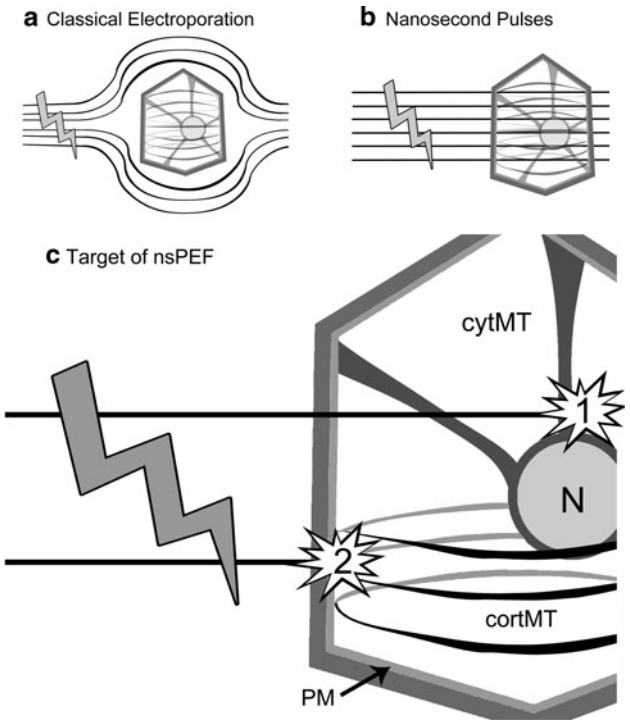

Fig. 5 Model for the site of action of pulsed electrical fields in plant cells. Classical electroporation uses pulses with low field strength and high duration. Such pulses are dissipated by charging of the cell membrane (**a**). Ultrashort nsPEFs with high field strengths and low durations are thought to penetrate into the cell interior and to affect intracellular targets before being dissipated by charging of the cell membrane (**b**). In this work we investigated the location of the cellular targets of nsPEFs. We show that in addition to intracellular targets (*1*) nsPEFs can specifically affect targets located at the plasma membrane (*2*) (**c**). *cytMT* cytoplasm microtubule, *corMT* cortical microtubule, *N* nucleus, *PM* plasma membrane

systems. In the current study we addressed this issue using a single experimental system but a target that is localized either in the cell interior or adjacent to the plasma membrane (Klotz and Nick 2012).

As cellular readout for the nuclear function of KCH, NP heralding the ensuing cell division was quantified (Frey et al. 2010). This movement depends on a perinuclear cage of actin filaments and microtubules that are linked by KCH kinesins. When this linkage is disturbed by overexpression of KCH, nuclear movement is delayed. Similarly, a mild nsPEF treatment was able to cause a similar delay. A combination of both factors acted synergistically. At first sight, this experiment suggests a site of action at the nucleus, i.e., in the cell interior. However, it should be kept in mind that the nucleus is tethered, through a radial network of actin filaments and microtubules, to the cell wall by means of transmembrane proteins (Pickard 2008). If the attachment of this radial network to the plasma membrane was disrupted by nsPEFs, this should result in a similar delay of nuclear migration. Thus, the analysis of nuclear migration is not sufficient.

We therefore made use of a second cellular function that is unequivocally linked to the cell periphery: cell expansion, which is controlled by a directional extensibility of the cell wall that, in turn, is regulated by the orientation of cortical microtubules binding a specific subset of KCH subtending the plasma membrane. In fact, we observed that (1) overexpression of KCH promoted cell expansion, (2) this promotion was stimulated by nsPEFs in the KCH overexpressor but not in the nontransformed wild type (i.e., in a strict synergy) and (3) the cell expansion responds more sensitively compared to cell division. These phenomena are specific for the membrane-associated cytoskeleton. Thus, whereas the observed effect on nuclear migration (and consequently mitotic activity) can be also explained by a site of action at the plasma membrane, it is not possible to explain the effect of nsPEFs on cell expansion by a site of action at the perinuclear cytoskeleton.

Due to its calponin-homology domain, KCH1 cross-links actin and microtubules as part of a signaling hub, which probably harbors a phospholipase D as an additional member. The nsPEFs probably act on this signaling hub, resulting in a release of microtubules from actin, which promotes alignment of microtubules in a transverse array of parallel bundles. This alignment requires microtubule detachment of the membrane (Sainsbury et al. 2008). The resulting reinforcement of transverse microtubule alignment is then transduced into a transverse orientation of cellulose microfibrils (the cellulase synthases move along microtubules), which provides the anisotropy of cell-wall extensibility required to sustain elongation of the expanding cell. All these processes driving cell elongation proceed to a certain extent also under control conditions; however, they are promoted by the nsPEFs and the overexpression of KCH1.

In the current work we made use of a protein (a plant-specific KCH) that exhibits two distinct functions depending on its localization either adjacent to the plasma membrane or at the nuclear envelope. We show that nsPEFs can cause a specific biological response produced by the cytoskeleton adjacent to the plasma membrane of plant cells. We cannot exclude that nsPEFs are also active at the cell center (although the observed effects can be understood as secondary from cytoskeletal perturbation at the plasma membrane), but our results showed a clear side of action of these ultrashort pulses at the membrane-associated cytoskeleton, even at very short pulse durations. Here, we used a dual target because the biological activity in two different locations, close to the membrane and at the perinuclear cage, enables one to observe two stories at the same time. For future studies, we have already proceeded and generated a transgenic line overexpressing the putative complex partner of submembraneous KCH, phospholipase D, acting exclusively at the plasma membrane.

Acknowledgments This work was supported by a fellowship of the Chinese Scholarship Council to Q. L. Rüdiger Wüstner (Karlsruhe Institute of Technology) is acknowledged for excellent technical assistance during nsPEF treatment and Sabine Purper (Karlsruhe Insitut of Technology), for competent cultivation of high-quality cell lines.

References

Alkhafaji SR, Fraid M (2007) An investigation on pulsed electric fields technology using new treatment chamber design. Innov Food Sci Emerg Technol 8(2):205–212

Beebe SJ, Fox PM, Rec LJ, Somers K, Stark RH, Schoenbach KH (2002) Nanosecond pulsed electric field (nsPEF) effects on cells and tissues: apoptosis induction and tumor growth inhibition. IEEE Trans Plant Sci 30(1):286–292

Beebe SJ, Fox PM, Rec LJ, Willis EL, Schoenbach KH (2003) Nanosecond high-intensity pulsed electric fields induce apoptosis in human cells. FASEB J 17:1493–1495

Belehradek M, Domenge C, Luboinski B, Orlowski S, Belehradek J Jr, Mir LM (1993) Electrochemotherapy, a new antitumor treatment. First clinical phase I-II trial. Cancer 2:3694–3700

Berghöfer T, Eing C, Flickinger B, Hohenberger P, Wegner L, Frey W, Nick P (2009) Nanosecond electric pulses trigger actin responses in plant cells. Biochem Res Commun 387:590–595

Breton M, Delemotte L, Silve A, Mir LM, Tarek M (2012) Transport of siRNA through lipid membranes driven by nanosecond electric pulses: an experimental and computational study. J Am Chem Soc 134:13938–13941

Brodelius PE, Funk C, Shillito RD (2005) Triggered Marx generators for the industrial-scale electroporation of sugar beets. IEEE Trans Ind Appl 3:186–188

Buescher ES, Schoenbach KH (2003) Effects of submicrosecond, high intensity pulsed electric fields on living cells—intracellular electromanipulation. IEEE Trans Dielectr Electr Insul 10: 5788–5794

Campanoni P, Blasius B, Nick P (2003) Auxin transport synchronizes the pattern of cell division in a tobacco cell line. Plant Physiol 133(3):1251–1260

Chang DC, Reese TS (1990) Changes in membrane structure induced by electroporation as revealed by rapid-freezing electron microscopy. Biophys J 58:1–12

Chen C, Smye SW, Robinson MP, Evans JA (2006) Membrane electroporation theories: a review. Med Biol Eng Comput 44:5–14

Eing C, Bonnet S, Pacher M, Puchta H, Frey W (2009) Effects of 1 nanosecond pulsed electric fields exposure on *Arabidopsis thaliana*. IEEE Trans Dielectr Electr Insul 16:1322–1328

Flickinger B, Berghöfer T, Hohenberger P, Eing C, Frey W (2010) Transmembrane potential measurements on plant cells using the voltage-sensitive dye ANNINE-6. Protoplasma 247:3–12

Ford WE, Ren W, Blackmore PF, Schoenbach KH, Beebe SJ (2010) Nanosecond pulsed electric fields stimulate apoptosis without release of pro-apoptotic factors from mitochondria in B16f10 melanoma. Arch Biochem Biophys 497:82–89

Frey N, Klotz J, Nick P (2009) Dynamic bridges—a calponin-domain kinesin from rice links actin filaments and microtubules in both cycling and non-cycling cells. Plant Cell Physiol 50(8): 1493–1506

Frey N, Klotz J, Nick P (2010) A kinesin with calponin-homology domain is involved in premitotic nuclear migration. J Exp Bot 61:3423–3437

Gaff DF, Okong'O-Ogola (1971) The use of non-permeating pigments for testing the survival of cells. J Exp Bot 22:756–758

Gimona M, Djinovic-Carugo K, Kranewitter WJ, Winder SJ (2002) Functional plasticity of CH domains. FEBS Lett 513:98–106

Gowrishankar TR, Esser AT, Vasilkoski ZV, Smith KC, Weaver JC (2006) Microdosimetry for conventional and supra-electroporation in cells with organelles. Biochem Biophys Res Commun 310:1266–1276

Hohenberger P, Eing C, Straessner R, Durst S, Frey W, Nick P (2011) Plant actin controls membrane permeability. Biochim Biophys Acta 1808:2304–2312

Hu Q, Joshi PR, Schoenbach KH (2005) Simultation of nanopore formation and phosphatidylserine externalization in lipid membranes subjected to a high-intensity, ultrashort electric pulses. Phys Rev E 72:031902

Ibey BL, Roth CC, Pakhomov AG, Bernhard JA, Wilmink GJ, Pakhomova ON (2011) Dose-dependent thresholds of 10-ns electric pulse induced plasma membrane disruption and cytotoxicity in multiple cell lines. PLoS ONE 6(1):e15642

Jovanovic AM, Durst S, Nick P (2010) Plant cell division is specifically affected by nitrotyrosine. J Exp Bot 61:901–909

Klotz J, Nick P (2012) A novel actin–microtubule cross-linking kinesin, NtKCH, functions in cell expansion and division. New Phytol 193:576–589

Korenbaum E, Rivero R (2002) Calponin homology domains at a glance. J Cell Sci 115:3543–3545

Kotnik T, Miklavcic D (2000) Analytical description of transmembrane voltage induced by electric fields on spheroidal cells. Biophys J 79:670–679

Maisch J, Nick P (2007) Actin is involved in auxin-dependent patterning. Plant Physiol 143:1695–1704

Nagata T, Nemoto Y, Hasezawa S (1992) Tobacco BY-2 cell line as the "HeLa" cell in the cell biology of higher plants. Int Rev Cytol 132:1–30

Nakamura M, Naoi K, Shoji T, Hashimoto T (2004) Low concentrations of propyzamide and oryzalin alter microtubule dynamics in *Arabidopsis* epidermal cells. Plant Cell Physiol 45:1330–1334

Nesin OM, Pakhomova ON, Xiao S, Pakhomov AG (2011) Manipulation of cell volume and membrane pore comparison following single cell permeabilization with 60- and 600-ns electric pulses. Biochim Biophys Acta 1808:792–801

Nick P (2010) Probing the actin–auxin oscillator. Plant Signal Behav 5(2):94–98

Nick P, Han MJ, An G (2009) Auxin stimulates its own transport by shaping actin filaments. Plant Physiol 151:155–167

Nuccitelli R, Pliquett U, Chen X, Ford W, Swanson JR, Beebe SW, Kolb JF, Schoenbach KH (2006) Nanosecond pulsed electric fields cause melanomas to self-destruct. Biochem Biophys Res Commun 343:351–360

Nuccitelli R, Chen X, Pakhomov AG, Baldwin HW, Sheikh S, Ren W, Osgood C, Swanson RJ, Kolb JF, Beebe SJ, Schoenbach KH (2009) A new pulsed electric field therapy for melanoma disrupts the tumor's blood supply and causes complete remission without recurrence. Int J Cancer 125(2):438–445

Pickard BG (2008) "Second extrinsic organizational mechanism" for orienting cellulose: modelling a role for the plasmalemmal reticulum. Protoplasma 233:1–29

Preuss ML, Kovar DR, Lee YR, Staiger CJ, Delmer DP, Liu B (2004) A plant-specific kinesin binds to actin microfilaments and interacts with cortical microtubules in cotton fibers. Plant Physiol 136:945–3955

Qin BL, Pothakamury UR, Barbosa-Canovas GV, Swanson BG (1996) Nonthermal pasteurization of liquid foods using high-intensity pulsed electric fields. Crit Rev Food Sci Nutr 36:603–627

Rosemberg Y, Korenstein R (1997) Incorporation of macromolecules into cells and vesicles by low electric field: induction of endocytotic-like processes. Bioelectrochem Bioenerg 42:275–281

Růžička K, Šimášková S, Duclercq J, Petrášek J, Zažímalová E, Simon S, Friml J, Van Montagu J, Benková E (2009) Cytokinin

regulates root meristem activity via modulation of the polar auxin transport. Proc Natl Acad Sci USA 106:4284–4289

Sainsbury F, Collings DA, Mackun J, Gardiner J, Harper JDI, Marc J (2008) Developmental orientation of transverse cortical microtubules to longitudinal directions: a role for actomyosin-based streaming and partial microtubule-membrane detachment. Plant J 56:116–131

Sano T, Higaki T, Oda Y, Hayashi T, Hazewasa S (2005) Appearance of actin microfilament "twin peaks" in mitosis and their function in cell plate formation, as visualized in tobacco BY-2 cells expressing GFP–fimbrin. Plant J 44:595–605

Schoenbach KH, Beebe SJ, Buescher ED (2001) Intracellular effect of ultrashort electrical pulses. Bioelectromagnetics 22:440–448

Schoenbach KH, Joshi RP, Chen C, Kolb JF, Chen N, Stacye M, Blackmore P, Buescher ES, Beebe SJ (2004) Ultrashort electrical pulses open a new gateway into biological cells. Proc IEEE 92:1122–1137

Schoenbach KH, Joshi RP, Beebe SJ, Baum CE (2009) A scaling law for membrane permeabilization with nanopulses. IEEE Trans Dielectr Electr Insul 16:1224–1235

Staempfli R (1958) Reversible breakdown of the excitable membrane of a Ranvier node. Ann Acad Brasil Ciens 30:57–59

Takaki K, Yamazaki N, Mukaigawa S, Fujiwara T, Kofujita H, Takahasi K, Narimatsu M, Nagane K (2007) Improvement of edible mushroom yield by electric stimulations. J Plasma Fusion Res 8:556–559

Tang L, Yao C, Sun C (2009) Apoptosis induction with electric pulses—a new approach to cancer therapy with drug free. Biochem Biophys Res Commun 390:1098–1101

Tekle E, Oubrahim H, Dzekunov SM, Kolb JF, Schoenbach KH, Chock PB (2005) Selective field effects on intracellular vacuoles and vesicle membranes with nanosecond electric pulses. Biophys J 89(1):274–285

Weaver JC, Chizmadzhev YA (1996) Electroporation. In: Polk C, Postow H (eds) Handbook of biological effects of electromagnetic fields, vol 2. CRC Press, Boca Raton, pp 247–274

Yao C, Mi Y, Hu X, Li C, Sun C, Tang J, Wu X (2008) Experiment and mechanism research of SKOV3 cancer cell apoptosis induced by nanosecond pulsed electric field. Conf Proc IEEE Eng Med Biol Sci 2008:1044–1047